OPEN ACCESS

SCICELL

RESEARCH PAPER

DRY SLIDING WEAR AND SURFACE MORPHOLOGICAL EXAMINATION OF AN ALUMINIUM MATRIX COMPOSITE REINFORCED WITH PALM KERNEL SHELL

Francis Odikpo Edoziuno[1]*, Benjamin Ufuoma Odoni[2], Francis Ireti Alo[3], Cynthia Chinasa Nwaeju[4]

[1,2]Department of Metallurgical Engineering, Delta State Polytechnic, P.M.B. 1030 Ogwashi-Uku, Nigeria.

[3]Department of Material Science and Engineering, Obafemi Awolowo University, Ile-Ife, Nigeria.

[4]Department of Mechanical Engineering, Nigeria Maritime University, Okerenkoko, Warri, Delta State, Nigeria.

* Corresponding Author's email: francisedoziuno@gmail.com, Tel. +234806 342 2650; Department of Metallurgical Engineering, Delta State Polytechnic, P.M.B. 1030 Ogwashi-Uku, Nigeria.

ABSTRACT

The wear resistance and microstructural features of aluminium AA6063 based composites reinforced with seven different mass fractions of palm kernel shell (PKS) particles (0, 2.5, 5, 7.5, 10, 12.5 & 15wt%) fabricated by stir-casting, were characterized using pin-on-disk tribometer, optical microscope and image analysis. Image analysis revealed both the particle size and shape descriptors for the composites microstructural features. The average grain sizes of all the composites were higher than that of the unreinforced AA6063 matrix. Wear test conducted under dry sliding condition show that the volume reduction and specific wear rate increased to a maximum at 5wt% PKS addition and then decreased to the lowest level at 10wt% PKS. Subsequent addition of PKS above 10wt% yielded a further increase in the composites volume loss and specific wear rate. Composite sample reinforced with 10wt% PKS exhibited wear resistance response better than that of the unreinforced alloy. Image analysis afforded a comprehensive understanding of the microstructural features of the composites which influenced their behaviours.

Keywords: ImageJ; Image analysis; dry sliding wear; AA6063; Palm Kernel Shell; Aluminium matrix composites.

INTRODUCTION

The aim of developing metal matrix composite is to combine the desirable properties of the metal such as lightweight, high ductility, electrical and thermal conductivities with the properties of the reinforcement such as low coefficient of thermal expansion, high stiffness, and strength with abrasion resistance to produce material with a combination of desired physical and mechanical properties [1]. Aluminium metal matrix composites (AMMCs) are engineered materials made by incorporating single or hybrid non-metallic reinforcement(s) into aluminium or its alloy to tailor the properties such as strength, hardness, stiffness, electrical and thermal conductivity and various other properties. AMMCs found applications in aerospace, automotive, defence, marine, thermal management, electrical and electronic as well as sports goods. Aluminium alloys 2000, 5000, 6000 and 7000 series are the most frequently utilised matrix in the fabrication of AMMCs [2, 3]. AMMCs offer high strength to weight ratio, improved thermal conductivity, abrasion/wear resistance, creep resistance, dimensional stability and exceptionally good stiffness-to-weight ratio. Also, they have better high temperature performance [4–8]. Aluminium AA6063 is a class of aluminium alloy 6000 series having silicon and magnesium as the major alloying elements. Their major areas of application are in the automobile and aeronautic industries.

Wear phenomenon could be described as a progressive loss of materials by solid surfaces in dynamic contact [9–12]. The wear of composite materials have been classified into abrasive wear, adhesive wear, fatigue wear, erosive wear, fretting wear, oxidative wear and corrosive wear, depending on the mechanism of materials removed from the surface of bodies in contact or relative motion [9, 10, 13, 14]. In a sliding wear process, materials are removed by the dynamic interaction of two surfaces in relative contact, resulting in dimensional loss and material's volume reduction [9].

Materials' physical and mechanical properties are derived from their microstructural characteristics [15]. The development and use of automatic image analyzing tools and techniques for determining microstructural characteristics of materials have greatly reduced the rigour and tediousness associated with manual techniques [16]. Image analysis is concerned with accurately quantifying the microstructural features. Quantitative analysis of materials' microstructural features can be achieved using image analysis software. Either optical or scanning electron microscope micrographs can be used during image analysis [17, 18]. More commercial software programs, such as Amira, Comsol multiphysics, imageJ, etc., are available for the analysis of microstructural features of engineering materials [19, 20]. Image analysis is generally concerned with the acquisition of quantitative information and description of various parameters of the microstructure of a material such as determination of percentage fraction of phases or phase quantities, grain size estimation, grain shape, circularity and spatial distribution of microstructural elements observed using microscopic techniques [19, 21]. Microstructures with similar descriptors have similar materials properties [22]. Circularity or roundedness, for instance, is calculated as a shape parameter index in the ImageJ software. This image analysis software program supports standard image processing functions such as logical and arithmetical operations between images, contrast manipulation, convolution, Fourier analysis, sharpening, smoothening, edge detection, and median filtering. It does geometric transformations such as scaling, rotation, and flips. The general steps for materials structural analysis involves; surface preparation (cutting, grinding, polishing and etching), microscopic examination and image acquisition, image processing, quantitative image analysis (size, shapes and distribution of grains) and interpretation of results [19]. Image analysis had been utilized by researchers to quantify and measure the concentration of surface discolouration in laser-nitrided titanium alloy surface using the colour threshold function [23], analysed and compare the structure of two construction steels [19], quantify and estimate the microstructural parameter of ferritic-martensite dual phase steel [21]. Leica Qwin image analysis system was used to measure pore structures and pore distribution in aluminium powder metallurgy alloy [24]. The experimental demonstration has found image analysis procedure to be very effective in the measurement of materials grain size, pore structures and distribution and recommended for application in the ceramic and metallic industries, especially in powder metallurgy sintering operations [12, 24–27].

There is a research-established correlation of materials' microstructure with wear loss and hardness. It was shown that microstructural characteristics affect wear behaviour of sintered steel [27]. Lower wear loss is found to correlate with higher hardness and superior microstructure (one having higher dendrite density).

Conversely, higher wear loss correlates with lower hardness and poor microstructure [23]. This paper describes an investigation of the dry sliding wear behaviour of aluminium AA6063 reinforced with particles of palm kernel shell and microstructural analysis of the optical micrograph using image analysis software package.

MATERIALS AND METHODS

Collection and Preparation of Reinforcement Material

Palm kernel shell was obtained from an oil mill in Agbor, Delta State, South-South of Nigeria. The collected palm kernel shell (PKS) were washed with warm water, dried in direct sunlight for two weeks and grinded to a fine powder using the normal grain (wheat, corn, beans, etc.) grinding machine at the Ogwashi-Uku market. Particle size analysis of the palm kernel shell particle was carried out in Metallurgical Engineering laboratory, Delta State Polytechnic, Ogwashi-Uku. 100g of the PKS was placed unto a set of sieves arranged in descending order of fineness and shaken for 15mins to achieve complete classification. The PKS particles retained beneath the 212μm sieve was utilized in the research. The powder PKS was used in the unashed and untreated condition, as some other researchers had investigated it as a reinforcement in the processed and treated conditions [28–30].

Production of Composite by Stir Casting

The metal matrix composite was fabricated in the metallurgical Engineering laboratory of Delta State Polytechnic, Ogwashi-Uku, using the stir casting method. The sample was produced by varying the weight per cent of the reinforcing material (PKS) particles in the range of 0 to 15 wt.% at 2.5 wt.% interval, while the balance is aluminium alloy AA6063 matrix. The aluminium alloy was charged into a preheated stainless steel melting pot placed in an electric resistance furnace. The furnace was heated to ±700 ºC for 3 h. The PKS particles were preheated to 50 ºC in an oven for 3 h before they were added to the molten aluminium to improve the wettability and harmonize the temperature. The furnace temperature was first raised to 750 ºC to melt the alloy completely and then cooled to 600 ºC to keep the melt in a semi-solid state. At this stage, the preheated palm kernel shell particles were added and mixed manually using a steel stirring rod according to [29, 31]. After manual mixing and homogenisation, the composite slurry was placed back in the furnace and reheated to a temperature of 750 ºC and then poured into a preheated cylindrical mild steel mould with the dimension of length 200 mm x 16 mm diameter. The unreinforced aluminium AA6063 was also cast and used as the control sample for comparison.

Dry Sliding Wear Test

The wear test was carried out at room temperature on a Pin-on-Disc tribometer under dry sliding condition. A 10N constant load (N) was applied on all the specimens with dimension 40mm x 10mm x 6mm while sliding distance varied during the test. The procedure during the wear test involved; determination of the initial weight of the specimen, inserting and fixing the specimen on the specimen holder, applying the constant load on the supporting rod so that the stylus pin made firm contact with the specimen, turning the electric motor on to rotate the disc for just 2000 revolution cycles at a rotation speed of 200rpm. The specimen is finally weighed and the sliding distance covered measured. During sliding wear test using pin-on-disc equipment, the sliding speed of the wear process is dependent on the revolution of the disc and the contact point between the pin and the centre of the disc [32]. Wear evaluation was carried out by expressing the friction effects in terms of material volume loss (mm³) as a function of the sliding distance and the applied load. The specific wear rate, (W_S) was computed from the test results/parameters using equation (1) [33]. The magnitude of wear resistance (W_R) given in equation (3) is determined by taking the inverse of wear rate [30, 34], equation (2).

$$W_S = \frac{Volume\ Loss}{Applied\ Load \times Sliding\ Distance} \tag{1}$$

$$Wear\ rate\ \left(mm^3/Nm\right) = \frac{Volume\ loss\ (mm^3)}{Sliding\ Distance\ (m)} \times 1000 \tag{2}$$

$$W_R = \frac{Sliding\ Distance\ (S)}{Volume\ Loss(V_{loss})} \times 1000 \tag{3}$$

Morphological Examination Using Optical Microscope

The samples for optical metallographic examination were prepared and optical microscopy (OM) was carried out following the procedure described in [19, 35]. The metallographic characterization was carried out at 640× magnification. It should be noted, that a major condition for accurate image analysis is correct surface preparation of metallographic samples so that individual microstructural features would be sufficiently contrastive during image analysis [16, 36]. Inadequate specimen's preparation and wrong choice of etching technique were identified as major problem in using image analysis to reveal microstructural features [26].

Image Analysis of the Microstructure

ImageJ software package was used for image processing and image analyses. This automatic image analysing software is capable of defining and counting object in the picture, analysing their surface, length, boundaries, moments, quantifying of grains and measurement of grain sizes, the volume fraction of phase and depositing the results of analyses to spreadsheet data files [18]. The following procedures with detailed description given in [22, 23, 37, 38] were applied in conducting the ImageJ analysis: firstly, the surface morphology of the composites and the unreinforced aluminium alloy samples was captured by an optical microscope and exported as a high-resolution micrograph. Then the high-resolution micrograph was imported in the ImageJ software for image analysis. Finally, various functions and tools in imageJ software program were employed for specific measurement and analysis. Flowchart of the detailed procedures for the Image analysis is given as a block diagram in figure 1.
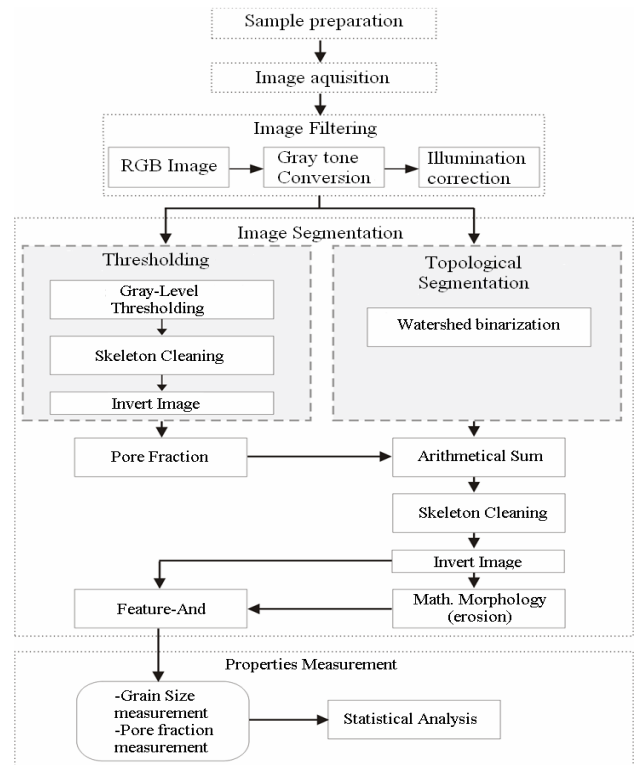

Fig. 1 Block diagram depicting the imageJ analysis procedure adapted from [25].

RESULTS AND DISCUSSION

Wear Behaviour of PKS/AA6063 Matrix Composites

The effects of reinforcement concentration applied normal load and sliding speed on the dry sliding wear properties (weight loss, volume loss, specific wear rate and wear resistance) are discussed in this investigation. Table 1 gives the result of the wear test and the sliding wear parameters. Graphical analysis of the influence of the reinforcement concentration (% weight fraction) on the specific wear rate, volume loss and wear resistance of the PKS reinforced aluminium alloy AA6063 matrix composites are given in Figures 2 – 7.

Table 1 Wear parameters and results of dry sliding wear test

Sample	Weight loss (g)	Sliding Distance (mm)	Volume Loss (mm³)	Specific Wear Rate (mm³/Nm)	Wear Resistance (mm/mm³)
Control	0.0015	3.4	0.79	0.27	4303.80
2.5% pks	0.0057	2.5	2.64	0.66	946.97
5% pks	0.0091	2.6	4.60	1.20	565.22
7.5%pks	0.0076	2.4	2.11	0.51	1137.44
10% pks	0.0009	2.4	0.53	0.13	4528.30
12.5% pks	0.0033	2.7	2.09	0.56	1291.87
15%pks	0.0031	2.8	2.33	0.65	1201.72

It could be readily observed from Table 1 that the weight loss of the composites increased as the reinforcement content increases to a maximum at 5% PKS and then decreased to a minimum at 10% PKS content. Despite that, the applied normal load was constant at 10N during the tribological test. Generally, the composites with higher per cent weight fraction of the reinforcement (10, 12.5 & 15%), recorded lower weight loss during the sliding wear experiment. While, those with lower content of the particulate reinforcement (2.5, 5 & 7.5%) have a higher loss in weight during wear test.

Considering the influence of the reinforcement concentration on the specific wear rate, and volume loss of the AA6063 matrix composites shown in Figures 2 & 3, it could be noticed that the volume reduction and specific wear rate increased to a maximum at 5wt% PKS content and then decreased to the lowest level at 10wt% PKS. Subsequent addition of PKS above 10wt% resulted in a further increase in the composites volume loss and specific wear rate. The composite sample reinforced with 10wt% PKS has a specific wear rate and volume loss far lower than that of the unreinforced alloy.
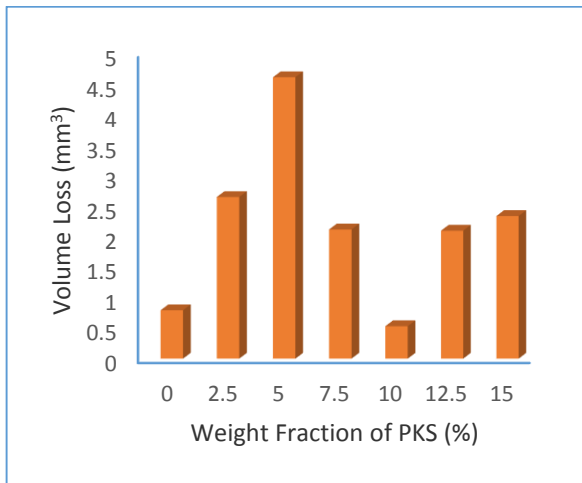

Fig. 2 Effect of concentration of PKS (wt%) on the volume loss (mm³) of AA6063 matrix composites during sliding wear test
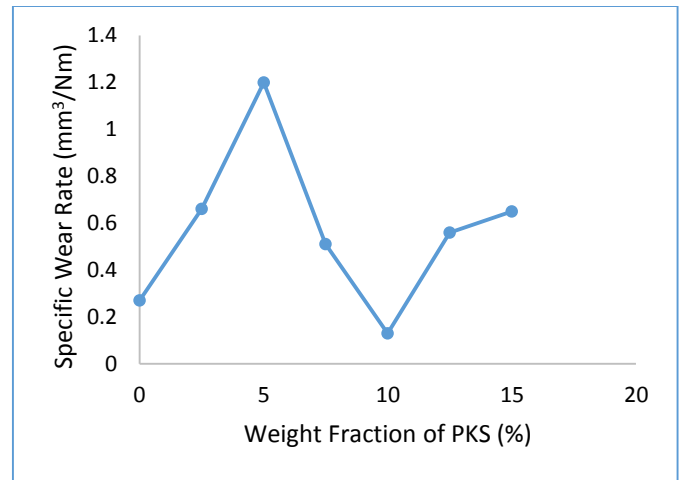

Fig. 3 Effect of concentration of PKS (wt%) on the specific wear rate (mm³/Nm) of AA6063 matrix composites during sliding wear test

The influence of the reinforcement weight content on the sliding distance covered during the dry sliding wear experiment is analysed in Figure 4. Evaluation of the figure revealed that the sliding distance covered reduced progressively from 3.5mm to 2.4mm, as PKS particles were added to the aluminium alloy matrix, despite that all the specimen were rotated just 2000 cycle at the rotation speed of 200rpm. This could be as a result of the frictional effect of the composites surface roughness, unlike the smooth-surfaced control sample. This is also corroborated by the average grain sizes of the microstructure obtained by image analysis (Table 2), which increased as more PKS were added to the AA6063 matrix. As expected, the composite sample reinforced with 10wt% PKS covered the lowest sliding distance during the abrasive sliding.
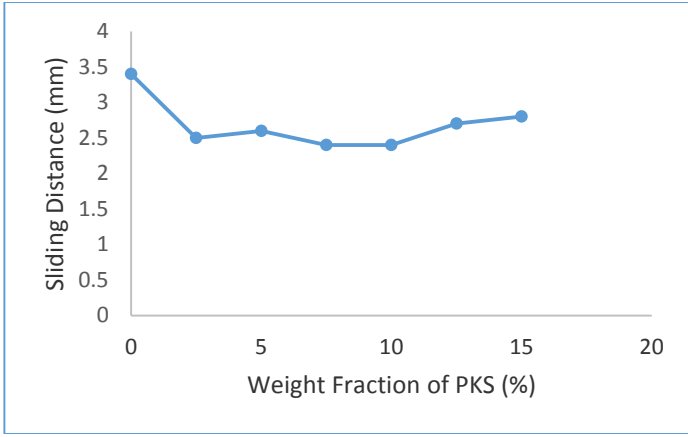
Fig. 4 Effect of concentration of PKS (wt%) on the sliding distance (mm) covered during sliding wear test

In figure 5 is depicted, the impact of reinforcement concentration (wt%) on the sliding wear resistance of the composites. All the composites samples have lower wear resistance than the unreinforced AA6063 alloy, except the 10wt% PKS reinforced sample. Maximum wear resistance was recorded at 10wt% PKS content.
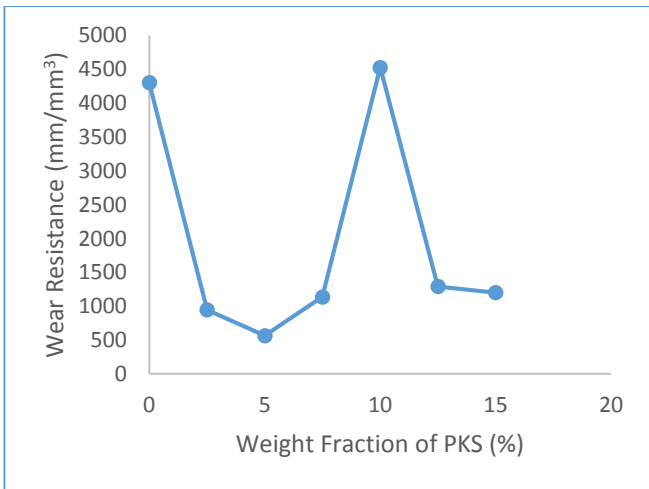

Fig. 5 Effect of concentration of PKS (wt%) on the wear resistance (mm/mm^3) of AA6063 matrix composites during sliding wear test

Image Analysis of PKS/AA6063 Matrix Composites

Relevant quantitative descriptors (stereological parameters) are used in characterizing the dimensional and morphological characteristicss of materials. The quantitative description of the microstructure involves the use of a set of numbers that define density, size, shape, and spatial arrangements (three-dimensional properties) of the microstructural features [22]. These quantitative descriptors are based on the theory of geometrical probability and can be obtained from measurements carried out on the microstructural image using specific functional tools of the image analysis software package. The most common quantitative microstructural measurement is that of the grain size of materials [22]. Analyze particle function was used to determine the perimeter, the grain counts, average size, %Area, circularity, solidity, etc. Composite sample reinforced with 15wt% PKS recorded the maximum count of grains, while the 5wt% PKS reinforced sample has the lowest grain count. The average particle sizes of 5, 7.5 and 15wt%PKS reinforced composites were higher than that of the unreinforced AA6063 matrix, which may correlate to the high wear rate observed for those reinforcement weight fractions. The quantitative results in Table 2 display the particle size descriptors, which were used to compute the various particle shape descriptors given in Table 3.

The circularity, a popular shape factor/parameter allows for evaluating the shape of grains. Circularity, C, is a dimensionless value, which can be used to estimate the degree to which the particle resembles a circle, with consideration of the smoothness of the perimeter. It is the ratio of the perimeter of a circle of the same area as the particle to the perimeter of the particle. This implies that circularity is a measurement of both the form and roughness of the particle. Thus, if a particle is not perfectly round, or a smooth circle, the circularity value will be lower [24, 39]. The shape descriptors in Table 3 revealed that the unreinforced aluminium alloy matrix has the highest value of circularity, closely followed by the 15wt% PKS reinforced composite. Feret's diameters characterize the particles outer horizontal and vertical dimensions; length and width (FeretX and FeretY). Aspect ratio, AR is defined as the ratio of the Feret's minimum length to the Feret's maximum length. Thus, as the width and length of the shape approach the same value, the aspect ratio approaches one [39]. This does not necessarily mean the shape is circular, though a perfect circle will have an aspect ratio of 1.0 [24]. Often, very symmetric shapes like square, regular octagon, equilateral triangle and symmetric cross, have a very high aspect ratio. Elongated shapes have lower values of aspect ratios [22]. From Table 3, the AR of the unreinforced alloy is higher than that of the PKS reinforced AA6063 matrix. It also has the lowest elongation ratio of 1.796. The highest elongation ratio of 2.153 was obtained by the composite sample reinforced with 7.5wt% PKS, which also have the lowest AR of 0.464. When a shape becomes less smooth or more irregular (or rougher), the perimeter of the shape may increase very quickly, depending on the size and number of the irregularities in the shape contributing to the roughness [39]. The irregularity of the unreinforced alloy was highest followed by the 7.5wt% PKS reinforced composite. Equivalent circle diameter (ECD) is the diameter of the circle having the same area as the area of the particle. Solidity, S, is a dimensionless value which measures the overall concavity of a particle. It can be defined as the image area, A, divided by the convex hull area, Ac. This implies that, as the particle becomes more solid, the image area and convex hull area tend to approach each other, resulting in a solidity value of unity. Conversely, as the particle shape digresses from a closed circle, the convex hull area increases and the computed solidity decreases. As a shape becomes rougher or less solid, the solidity value will approach zero. Conversely, shapes that are very smooth, and rounded have solidity values that approach one. From Table 3, the shape of the particles of the composite reinforced with 7.5%PKS is more rounded than other samples.

Table 2 Summary of Image Analysis Results of Particle Size (Size Descriptors) for AA6063/PKS Composites and the Unreinforced AA6063

Sample	Slice	Grain Count	Total Area	Average Size(μm)	% Area (A)	Perimeter (P)	Feret (F)	FeretX	FeretY	Feret Ange	MinFeret (mF)
Control	Black & White Threshold	546	33476	61.311	45.272	34.731	6.126	148.354	106.147	120.482	3.411
5wt% PKS	Black & White Threshold	433	27003	62.363	41.372	38.704	8.849	147.083	125.353	128.681	4.184
7.5wt%PKS	Black & White Threshold	481	37852	78.694	45.946	39.593	7.834	147.981	143.657	117.873	3.638
15wt% PKS	Black & White Threshold	758	50341	66.413	40.861	27.847	6.869	176.017	165.468	136.986	3.281

Table 3 Microstructural Parameters and Shape Descriptors of AA6063/PKS Composites and the Unreinforced AA6063 Obtained from the Image Analysis Results

Sample	Circularity	Irregularity	Solidity	Aspect Ratio (AR)	Elongation Ratio (ER)	ECD
Control	0.797	5.611	0.83	0.557	1.796	7.592

5wt% PKS	0.742	4.374	0.796	0.473	2.115	7.258
7.5wt%PKS	0.772	5.054	0.845	0.464	2.153	7.649
15wt% PKS	0.786	4.054	0.827	0.478	2.094	7.213

ECD is equivalent circle diameter.

Figure 6a-d show the original images of AA6063, AA6063/5wt% PKS, AA6063/7.5wt% PKS and AA6063/15wt% PKS composites taken with metallurgical Optical microscope. The composites photomicrographs (Figure 6c-d) show a good dispersion of the PKS particulate reinforcement in the Al-Mg-Si

alloy matrix with small areas of reinforcement particles agglomeration, which characterizes stir-cast metal matrix composites [40]. There are areas of discolouration observable in the original optical micrographs running across grain boundaries and masking the microstructural features of the base alloy and composites (Figure 6). Image processing (image- colour adjust and threshold, noise elimination) of the original micrographs, produced a uniform surface colour in the images and reveal contrastive microstructural features (Figures 7 & 8).
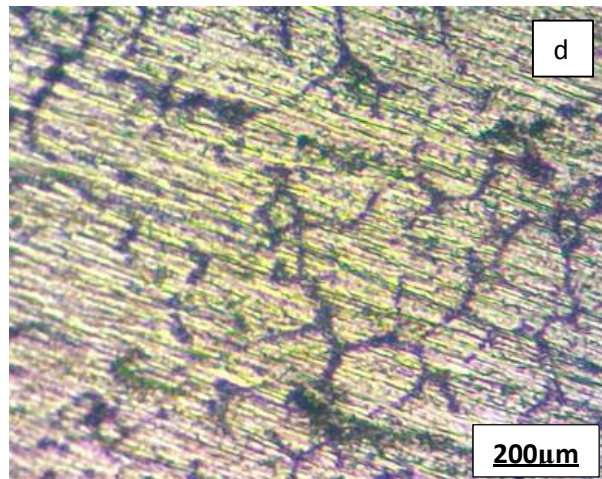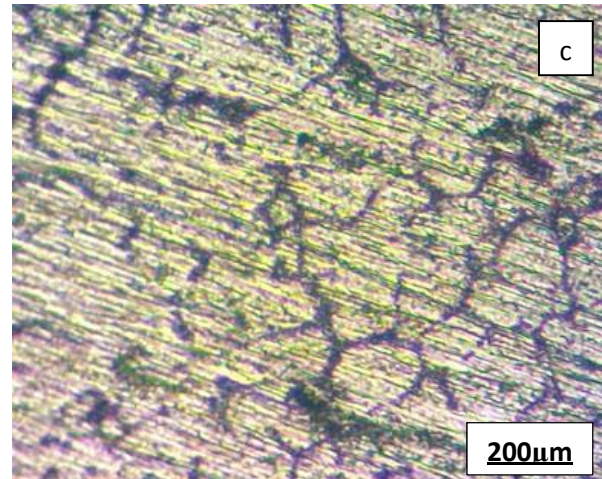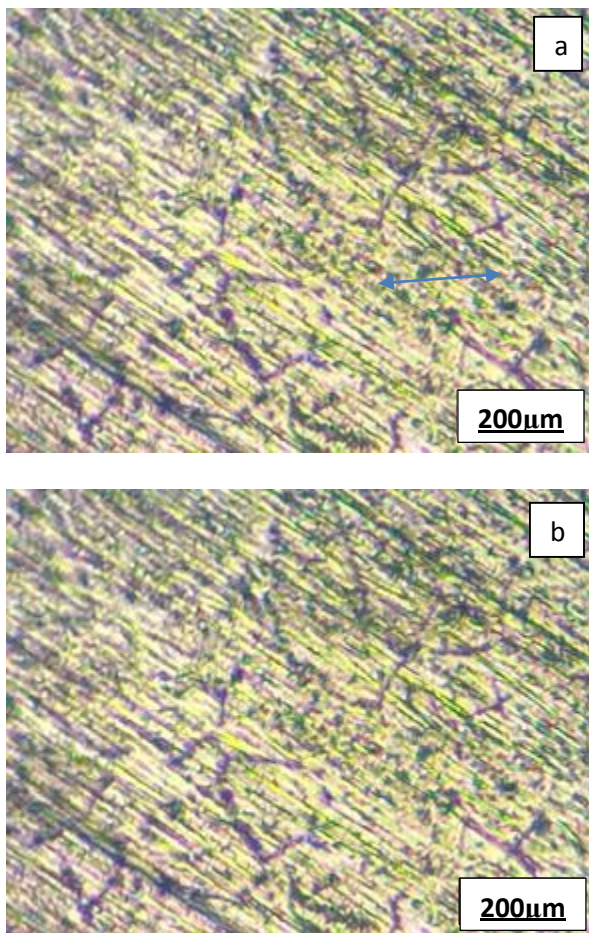

Fig. 6 Original optical micrographs of (a) Unreinforced AA6063, (b) AA6063/5wt%PKS, (c) A6063/7.5wt%PKS and (d) AA6063/15wt%PKS Composites at 640× magnification

Automatic thresholding is an important parameter in image analysis used to determine the division and segment between grains and grain boundaries. Threshold function is applied to determine the surface fraction indicated by the ratio of colour to the general surface of the entire image. According to ASTM standards E112-96 and E1382-97 requirements, the threshold is adjusted to detect either the grain interior or grain boundaries [16, 36]. Figures 7 & 8 reveal the processed and thresholded images of the reinforced and unreinforced AA6063 alloy. To obtain an image with a clear and accurate segmentation of grains and grain boundaries, the processed and thresholded images of Figure 7 were further subjected to noise elimination and conversion to binary form (black and white threshold), which is useful for subsequent quantitative and qualitative measurements during image analysis and microstructural descriptions. Small particles or matrix inside the grains are considered noise and must be eliminated. It could be observed that the grains of the micrographs in Figure 8 occupy differentiated homogenous area after noise elimination. There is the precipitation of larger, contrasting and more rounded grain sizes, especially in Figure 8d. Figure 10 reveals the phase fraction or volume of the shaded area, which are shown quantitatively in Table 2 as the % Area. It shows the particle distribution in both the reinforced and unreinforced matrix. While Figure 9a-d depict the interactive 3D surface plot of the particle distribution. The colour intensity on the 3D surface plot gives a graphic vision and description of the observed surface morphology of the composites [19].
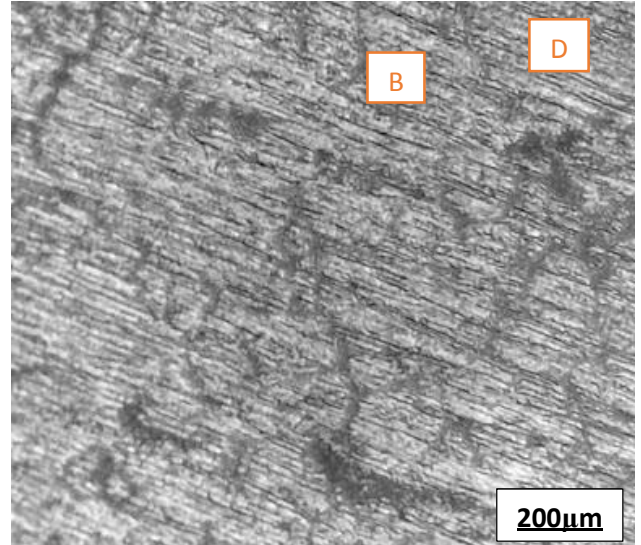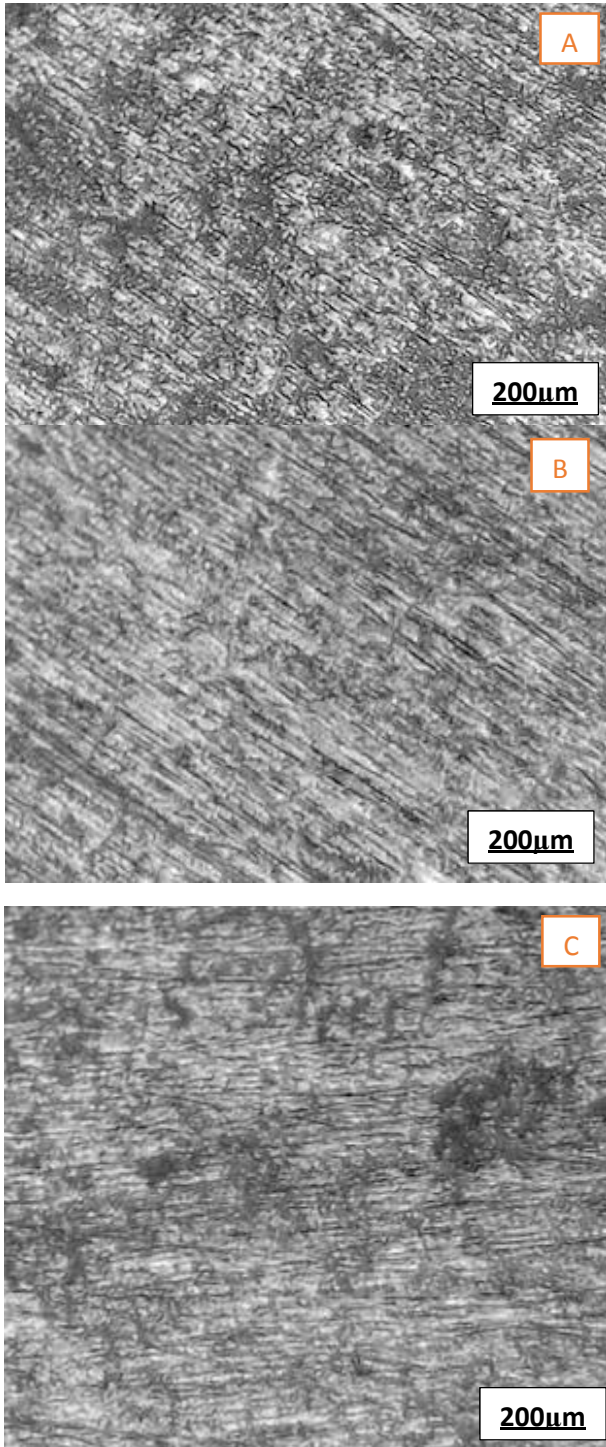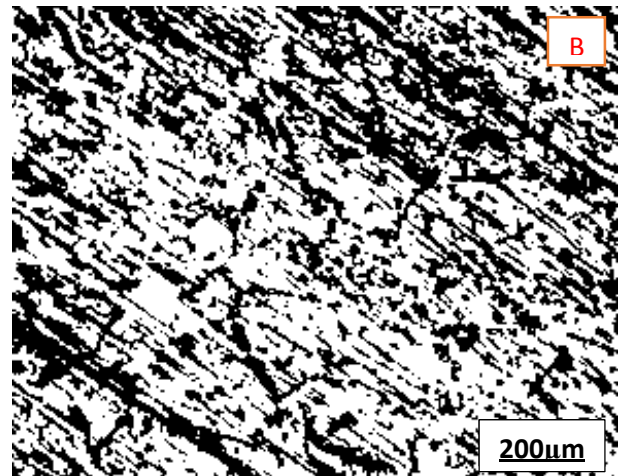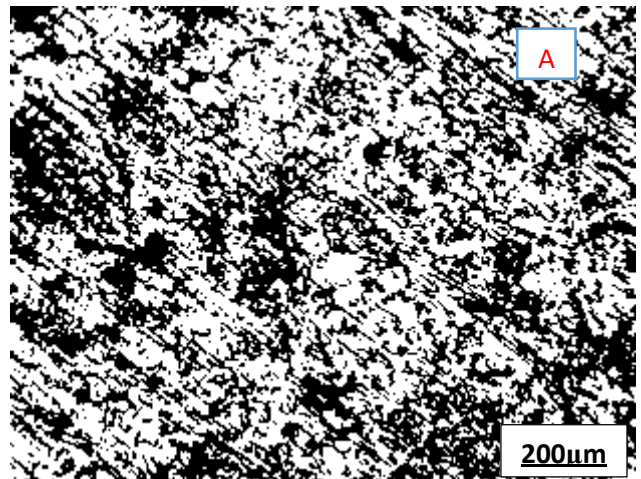
Fig. 7 Processed and threshold colour images (blue) after eliminating noise using the image analysis (a) Unreinforced AA6063, (b) AA6063/5wt%PKS, (c) A6063/7.5wt%PKS and (d) AA6063/15wt%PKS Composites
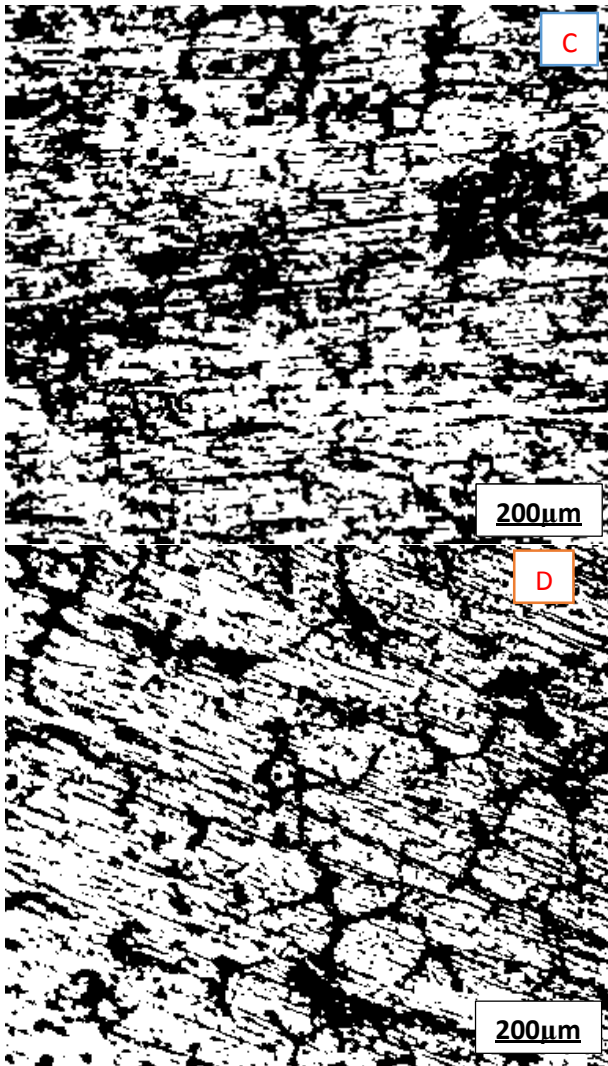
Fig. 8 Processed and thresholded (black and white) images (a) Unreinforced AA6063, (b) AA6063/5wt%PKS, (c) A6063/7.5wt%PKS and (d) AA6063/15wt%PKS Composites
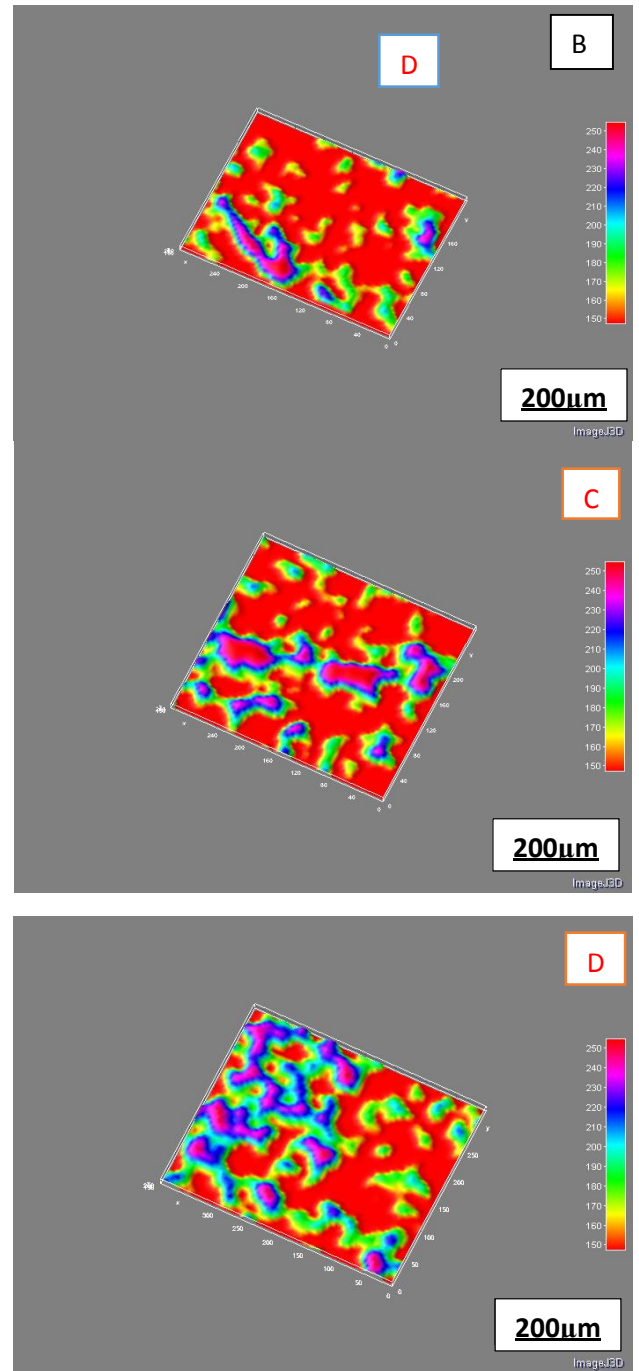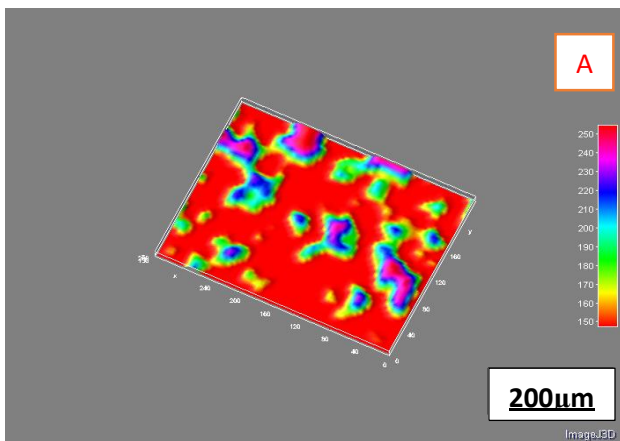

Fig. 9 Interactive 3D surface plot of (a) Unreinforced AA6063, (b) AA6063/5wt%PKS, (c) A6063/7.5wt%PKS and (d) AA6063/15wt%PKS Composites
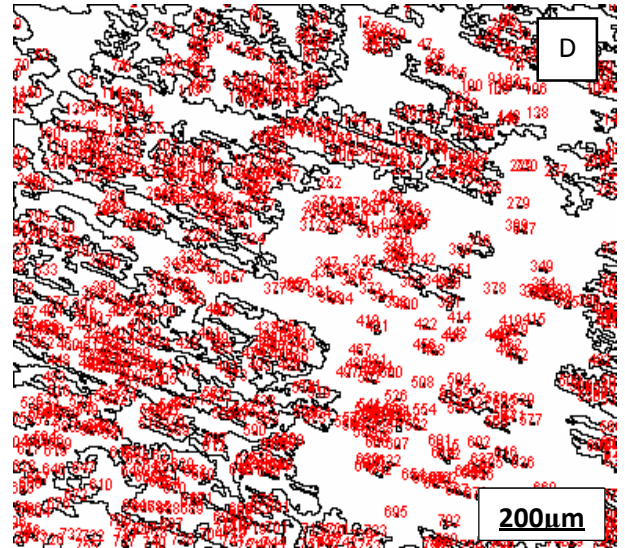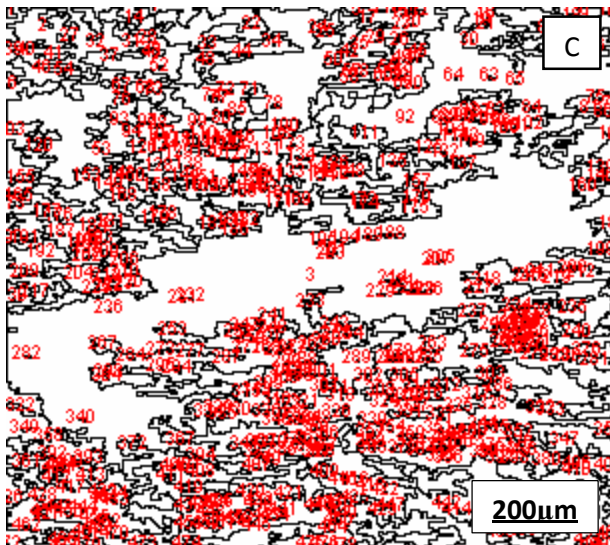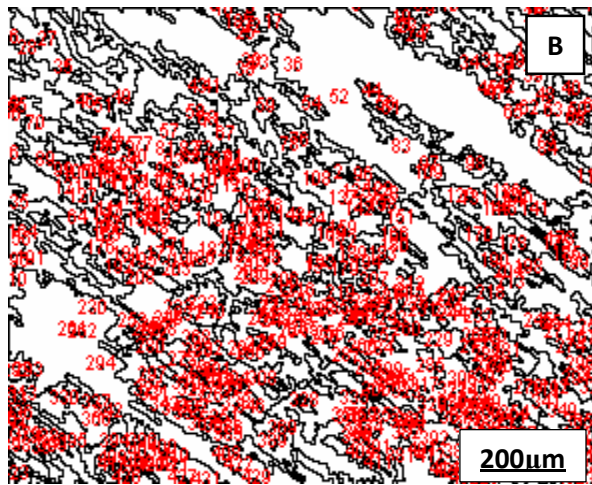
Fig. 10 Map drawing of the particle area distribution of black and white threshold (using Analyse tool) for (a) Unreinforced AA6063, (b) AA6063/5wt%PKS, (c) A6063/7.5wt%PKS and (d) AA6063/15wt%PKS Composites
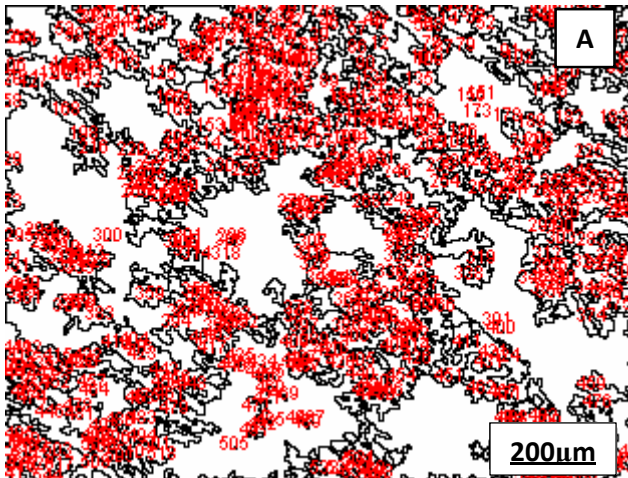
CONCLUSION

From the foregoing observations and analysis, it would be proper to conclude that better and enhanced wear properties were obtained by the 10wt% PKS reinforcement. The least sliding distance was covered in that sample during the abrasive sliding experiment due to higher surface friction opposing the sliding motion, despite the application of constant load and uniform number of cycles of revolution. It is shown that image analysis tools are useful for the assessment of microstructural features, such as particles size and shape descriptors and properties of aluminium matrix composites. Several particles shape and size factors were employed to sufficiently describe the non-spherical particles of the reinforced composites having some degree of roughness.

REFERENCES

1. Akaluzia, R.O., Edoziuno, F.O., Adediran, A.A., Odoni, B.U., Edibo, S., Olayanju, T.M.A.: Evaluation of the effect of reinforcement particle sizes on the impact and hardness properties of hardwood charcoal particulate-polyester resin composites. Materials Today: Proceedings, 2020. https://doi.org/10.1016/j. matpr.2020.02.980

2. Sanjay, M.R., Arpitha, G.R., Naik, L.L., Gopalakrisha, K., Yogesha, B.: Applications of Natural Fibers and Its Composites : An Overview. Natural Resources, 7, 2016, 108–114. https://doi.org/10.4236/nr.2016.73011

3. Rao, V.R., Chowdary, J.R., Balaji, A., Krishna, D.S., Bhavabhuthi, B.P.R., Sreevatsava, G., Abhiram, K.: A Review on Properties of Aluminium Based Metal Matrix Composites via Stir Casting. International Journal of Scientific & Engineering Research, 7(2), 2016, 742–749.

4. Dasgupta, R.: Aluminium Alloy-Based Metal Matrix Composites : A Potential Material for Wear Resistant Applications. ISRN Metallurgy 2012, 2012, 594573 . https://doi.org/10.5402/2012/594573

5. Babalola, P.O., Bolu, C.A., Inegbenebor, A.O., Odunfa, K.M.: Development of Aluminium Matrix Composites : A review. Online International Journal of Engineering and Technology Research, 2, 2014, 1–11.

6. Muley, A. V, Aravindan, S., Singh, I.P.: Nano and hybrid aluminum based metal matrix composites : an overview. Manufacturing Review, 2(15), 2015. https://doi.org/10.1051/mfreview/2015018

7. Dinesh, M., Ravindran, R.: Aluminium AA 7075 properties enhanced by Zirconium and Chromium nano particle. International Journal of ChemTech Research, 9(01), 2016, 296–301.

8. Bodunrin, M.O., Alaneme, K.K., Chown, L.H.: Aluminium matrix hybrid composites : a review of reinforcement philosophies ; mechanical , corrosion and tribological characteristics. Journal of Materials Research and Technology, 4(4), 2015, 434–445. https://doi.org/10.1016/j.jmrt.2015.05.003

9. Gaurav, A., Amar, P., Rajesh, K.S.: Parametric Optimization and Three-Body Abrasive Wear Behavior of Sic Filled Chopped Glass Fiber Reinforced Epoxy Composites. International Journal of Composite Materials, 3(2), 2013, 32–38. https://doi.org/10.5923/j.cmaterials.20130302.02

10. Suresha, B., Siddaramaiah, Kishore, Seetharamu, S., Kumaran, P.S.: Investigations on the influence of graphite filler on dry sliding wear and abrasive wear behaviour of carbon fabric reinforced epoxy composites. Wear, 267, 2009, 1405–1414. https://doi.org/10.1016/j.wear.2009.01.026

11. Moghadam, A.D., Omrani, E., Menezes, P.L., Rohatgi, P.K.: Mechanical and tribological properties of self-lubricating metal matrix nanocomposites reinforced by carbon nanotubes (CNTs) and graphene – A review. Composites Part B, 2015. https://doi.org/10.1016/j.compositesb.2015.03.014

12. Bidulsky, R., Grande, M.A., Dudrova, E., Kabatova, M., Bidulska, J.: Dry sliding wear behaviour of low alloyed sintered steels in relation to microstructure and fracture behaviour. Powder Metallurgy, 59(2), 2016, 121–127. https://doi.org/10.1179/1743290115Y.0000000022

13. Ashok Kumar, R.T., Mohan, N., Mahesha, C.: Sliding Wear Characteristics of Fiber Reinforced Fillers Filled Polymer Based Composites : A Review. International Journal of Materials Science, 10(2), 2015, 133–169.

14. Wang, B.C., He, H., He, X.F., Chen, H.D., Huang, B.: Wear resistance , oil resistance , morphology and vulcanization performances of ethylene-vinyl acetate / acrylonitrile butadiene rubber composites. Express Polymer Letters, 13(12), 2019, 1088–1103. https://doi.org/10.3144/expresspolymlett.2019.94

15. Wang, M.Y., Williams, J.J., Jiang, L., Carlo, F. De, Jing, T., Chawla, N.: Three Dimensional (3D) Microstructural Characterization and Quantitative Analysis of Solidified Microstructures in Magnesium-Based Alloys. Metallogr. Microstruct. Anal. 1, 2012, 7–13. https://doi.org/10.1007/s13632-012-0008-x

16. Vander Voort, G.F.: *Metallography: Principles and Practice*. ASM International, Philadelphia, 1999.

17. Erisir, E., Bilir, G.O.: *Quantitative Analysis of Microstructure Constituents of Dual Phase Steels*. In: Proceedings of the 2nd International Iron and Steel Symposium (IISS'15). , Karabuk, 2015.

18. Kipanyula, M.J., Sife, A.S.: Global Trends in Application of Stereology as a Quantitative Tool in Biomed Research. Biomedical Research International. 2018, 2018, 1825697. https://doi.org/10.1155/2018/1825697

19. Alo, F.I., Ajoge, E.O., Kunle, M.O., Isadare, D.A., Oyedele, A.A., Emordi, N.: Comparision of Imagej Analysis of Structure of Two Constructional Steel. American Journal of Engeering & Applied Sciences. 1(1), 2018. https://doi.org/10.3844/ajeassp.2018

20. Rishi, N.R.: Particle Size and Shape Analysis using Imagej with Customized Tools for Segmentation of Particles. International Journal of Engeering Research & Technology. 4(11), 2015, 247–250.

21. Burikova, K., Rosenberg, G.: *Quantification of Microstructural Parameter Ferritic-Martensite Dual Phase Steel by Image Analysis*. In.: METAL 2009 - 18th International Conference on Metallurgy and Materials, Conference Proceedings2009, 185-189.

22. ASM: Practical Guide to Image Analysis. ASM International, Philadelphia, 2000.

23. Chan, C.-W., Lee, S., Smith, G.C., Donaghy, C.: Fibre Laser Nitriding of Titanium and its Alloy in Open Atmosphere for Orthopaedic Implant Applications : Investigations on Surface Quality, Microstructure and Tribological Properties. Surface Coatings Technology, 309, 2017, 628–640. https://doi.org/10.1016/j.surfcoat.2016.12.036

24. Bidulská, J., Kvačkaj, T., Kočiško, R., Bidulský, R., Grande, M.A., Donič, T., Martikan, M.: Influence of ECAP-Back Pressure on the Porosity Distribution.

25. Diogenes, A.N., Hoff, E.A., Fernandes, C.P.: Grain size measurement by image analysis : An application in the ceramic and in the metallic industries. In: Proceedings of the 18th International Congress of Mechanical Engineering. , Ouro Preto, 2005.

Acta Physica Polonica A, 117(5), 2010, 864–868. https://doi.org/10.12693/APhysPolA.117.864

26. Bidulska, J., Bidulsky, R., Grande, M.A., Kvackaj, T.: Different Formation Routes of Pore Structure in Aluminum Powder Metallurgy Alloy. Materials, 12(22), 2019, 3724. https://doi.org/10.3390/ma12223724

27. Bidulsky, R., Grande, M.A., Bidulska, J., Vlado, M., Kvackaj, T.: Wear Mechanism of Chromium Pre-Alloyed Sintered Steel. High Temperature Materials and Processes, 28(3), 2009, 175–180. https://doi.org/10.1515/HTMP.2009.28.3.175

28. Oladele, I.O., Ibrahim, I.O., Adediran, A.A., Akinwekomi, A.D., Adetula, Y. V, Olayanju, T.M.A.: Modified palm kernel shell fiber / particulate cassava peel hybrid reinforced epoxy composites. Results in Materials, 5, 2020, 100053. https://doi.org/10.1016/j.rinma.2019.100053

29. Oladele, I.O., Okoro, A.M.: The effect of palm kernel shell ash on the mechanical properties of as-cast aluminium alloy matrix composites. Leonardo Journal of Science, Jan-June, 2016, 15–30.

30. Ikumapayi, O.M., Akinlabi, E., Akinlabi, S.A.: Characterization of high strength aluminium – based surface matrix composite reinforced with low-cost PKSA fabricated by friction stir processing. Materials Research Express, 6, 2019. https://doi.org/10.1088/2053-1591/ab395b

31. Edoziuno, F.O., Adediran, A.A., Odoni, B.U., Utu, O.G., Olayanju, A.: Physico-chemical and morphological evaluation of palm kernel shell particulate reinforced aluminium matrix composites. Materials Today: Proceedings, 2020. https://doi.org/10.1016/j.matpr.2020.03.641

32. Hariharasakthisudhan, P., Rajan, S.B., Sathickbasha, K.: Inspiration of reinforcements , manufacturing methods , and microstructural changes on wear behavior of metal matrix composites – a recent review. Materials Research Express, 2020. https://doi.org/10.1088/2053-1591/ab6918

33. Nicolais, L., Meo, M., Milella, E. eds: Composite Materials - A Vision for the Future. Springer-Verlag, London, 2011.

34. Friedrich, K., Zhang, Z., Schlarb, A.K.: Effects of various fillers on the sliding wear of polymer composites. Composite Science and Technology, 65, 2005, 2329–2343. https://doi.org/10.1016/j.compscitech.2005.05.028

35. Orhadahwe, T.A., Adeleke, A.A., Aweda, J.O., Ikubanni, P.P., Odusote, J.K.: Microstructural image analysis of mild carbon steel subjected to rapid cyclic heat treatment. Journal of Chemical Technology and Metallurgy, 55, 2020, 198–209.

36. Peregrina-barreto, H., Terol-villalobos, I.R., Rangel-magdaleno, J.J., Herrera-navarro, A.M., Morales-hernandez, L.A., Manriquez-Guerrero, F.: Automatic grain size determination in microstructures using image processing. Measurement, 46, 2013, 249–258. https://doi.org/10.1016/j.measurement.2012.06.012

37. Chan, C., Smith, G.C.: Fibre laser joining of highly dissimilar materials : Commercially pure Ti and PET hybrid joint for medical device applications. Materials Design, 103, 2016, 278–292. https://doi.org/10.1016/j.matdes.2016.04.086

38. Goriewa-duba, K., Duba, A., Wachowska, U., Wiwart, M.: An Evaluation of the Variation in the Morphometric Parameters of Grain of Six Triticum Species with the Use of Digital Image Analysis. Agronomy, 8, 2018, 296. https://doi.org/10.3390/agronomy8120296

39. Olson, E.: Particle Shape Factors and Their Use in Image Analysis – Part 1 : Theory. Journal of GXP Compliance, 15(3), 2011.

40. Alaneme, K.K., Oganbule, C.A., Adewale, A.: Circumferential Notch Test Based Fracture Toughness Investigation of Al-Mg-Si Alloy Composites Reinforced with Alumina and Quarry Dust. Journal of Chemical Technolology and Metallurgy, 55, 2020, 469–478.